Journal of Applied Electrochemistry **33**: 1035–1042, 2003.

Electrodeposition and characterization of thin layers of Zn–Co alloys obtained from glycinate baths

S.M. RASHWAN[1,*], A.E. MOHAMED[1], S.M. ABDEL-WAHAAB[2] and M.M. KAMEL[1]
[1]*Chemistry Department, Faculty of Science, Suez Canal University, Ismailia, Egypt*
[2]*Chemistry Department, Faculty of Science, Ain Shams University, Cairo, Egypt*
*(*author for correspondence)*

Received 24 July 2002; accepted in revised form 4 April 2003

Key words: electrodeposition, glycinate baths, steel substrates, thin layers, Zn–Co alloys

Abstract

An alkaline bath containing $CoSO_4 \cdot 7H_2O$, $ZnSO_4 \cdot 7H_2O$, Na_2SO_4 and NH_2CH_2COOH is proposed for the deposition of thin layers of Zn–Co alloys onto steel substrates. Electrodeposition was carried out at 0.216–1.080 A dm^{-2}, pH 10 and 10–55 °C. The influence of bath composition, current density and temperature on galvanostatic cathodic polarization, cathodic current efficiency and alloy composition was studied. Different proportions of the two metals were obtained by using different deposition parameters, but at all Zn(II)/Co(II) ratios studied, preferential deposition of zinc occurred and anomalous codeposition took place. Increasing the bath temperature enhanced the cobalt content in the deposit. X-ray diffraction measurements indicated that the phase structure of the deposits was controlled by the applied current density. The Co_5Zn_{21} phase was formed at low current density, while the $CoZn_{13}$ phase was formed at high current density. The potentiodynamic dissolution of the coatings showed that they contained Zn–Co alloy of different content and structure.

1. Introduction

The electrodeposition of zinc–cobalt alloys is of great interest because these alloys exhibit significantly higher corrosion resistance than pure zinc [1–3]. Coatings with low Co content are less noble than steel and act as sacrificial coatings. Those with high Co content are nobler than steel and provide a barrier type of protection [4]. Compared with pure zinc, the coatings also have other favourable properties, for instance, hardness, ductility, internal stress, paintability and weldability. As characterized by Brenner [5], the electrodeposition of Zn–Co alloys from aqueous baths is of the anomalous type: that is, the less noble component, zinc, deposits preferably with respect to the more noble cobalt. Because of this, the cobalt content in the zinc–cobalt alloys produced from aqueous baths is usually low.

Zn–Co alloy coatings have been deposited from both simple and complex ions, typically in acid and alkaline baths, respectively. Okuda and Himatsu [6] produced a highly corrosion resistant Zn–Co alloy from acidic bath. Fratesi and coworkers [7] electrodeposited Zn–Co alloys on iron substrate from chloride bath. Highly adherent Zn–Co electroplates, fine grained with metallic luster were deposited onto steel substrates from acidic citrate bath by Abd El-Rehim et al. [8]. Bright and smooth Zn–Co alloy deposits with cobalt content ranging between 0.6–0.8% were obtained by Tu et al. [9]. Narasimhamurthy and Sheshadri [10] electrodeposited Zn–Co alloy from an alkaline sulfate bath containing triethanolamine and gelatin. These were smooth, uniform, and compact. They reported that the electrodeposition of Zn–Co alloys belongs to the anomalous type.

The majority of metal electrodeposition processes are carried out from baths containing complexing agents. Recently, various complexing agents such as fluoborates, sulfamates, tartrates, citrates, glycinates and gluconates have been used. These complexing agents are nontoxic, easily obtained and, upon degradation, effluent treatment is easier.

The aim of the present work was to carry out a systematic study of the elecrodeposition of Zn–Co alloys from glycinate baths. It deals with the effects of some plating variables on the cathodic polarization, cathodic current efficiency and composition of the deposits.

2. Experimental details

Zn–Co alloys were obtained under different conditions using baths of the following composition: 0.004–0.107 M $CoSO_4 \cdot 7H_2O$, 0.003–0.174 M $ZnSO_4 \cdot 7H_2O$, 0.14 M Na_2SO_4 and 1.33–1.86 M NH_2CH_2COOH. The solutions were prepared using distilled water and reagent

grade chemicals. The pH was adjusted using sulfuric acid or sodium hydroxide and measured by using a Fisher Scientific pH meter.

The experimental set-up consisted of a Perspex rectangular cell containing 50 cm^3 of electrolyte solution. The cathode was a 2.5 cm × 3.0 cm steel plate of composition: C 0.08%, Si 0.01%, Mn 0.3%, P 0.025% and Al 0.045%; the anode was a platinum sheet. The cathode was mechanically polished with progressively finer grades of emery paper and prior to deposition, it was washed with distilled water, and ethanol then it dried and weighed. The experiments were conducted at the required temperatures with the help of an air thermostat ±1 °C. The plating time was 15 min., after which the cathode was withdrawn, washed with distilled water, dried and weighed. The composition of each alloy was determined by means of a Perkin–Elmer 2380 atomic absorption spectrophotometer. This followed the dissolving of the deposited alloy by digestion in hydrochloric acid (32%) and diluting the solution with distilled water to 100 ml.

The galvanostatic cathodic polarization measurements were conducted in a three electrode cell, provided with a steel cathode rod of an area of 0.785 cm^2 of the same composition as mentioned above. A platinum wire was used as an anode and a saturated calomel electrode (SCE) as a reference electrode. The potential of the working electrode was measured via a potentiometer (Sargant Welch Scientific Co, USA). The polarization cell was cleaned and filled with 150 ml of the plating solution. The three electrodes were then inserted in their appropriate positions. The current is applied (2 mA increments) and the corresponding potential was measured.

The anodic stripping measurements were made in the above cell, where the working electrode was a glassy carbon disc of an area of 0.196 cm^2. The counter electrode was a platinum wire together with a saturated calomel electrode (SCE). The two electrodes were connected to a potentiostat (model 273) and X–Y recorder (model RE 0091).

The deposited phases were analysed by Siemens D 500 X-ray diffractometer at 35 kV and 15 mA, and identified by powder diffraction file card (JCPDS).

3. Results and discussion

3.1. *Galvanostatic cathodic polarization*

Figure 1 displays the galvanostatic cathodic polarization curves for the electrodeposition of pure cobalt (a), pure zinc (b) and Zn–Co alloy (c) in baths containing glycine under similar conditions. The figure shows that the individual discharge of each metal is accompanied by large polarization due to complex formation. The experimental polarization curve of Co lies at considerable more positive potentials than that of Zn deposition. This indicates that Co is the nobler metal in the present system. The polarization curve of the alloy lies between those of the parent metals. This suggests that the codeposition enables the less noble metal to codeposit at less cathodic potentials and causes the more noble metal to deposit at more cathodic potentials than in the individual deposition cases [11]. The given data suggest that in alloy deposition, cobalt would be deposited much more readily than zinc. This suggestion does not agree with the results obtained in the present work.

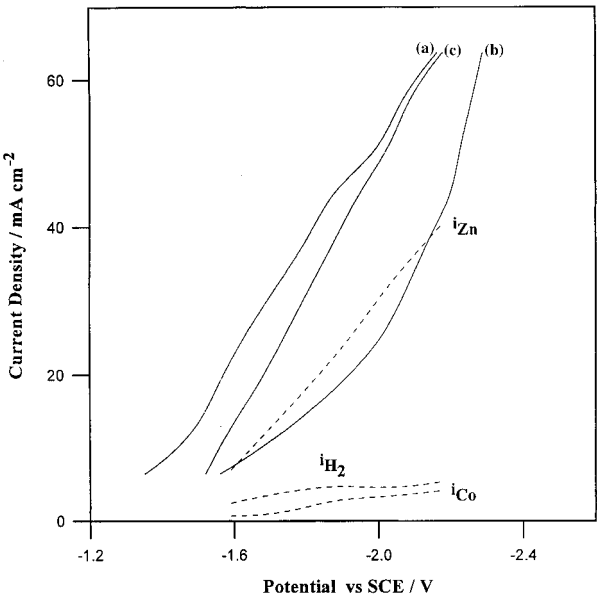

Fig. 1. Galvanostatic cathodic polarization curves (——) obtained at pH 10 and 25 °C for the electrodeposition of (a) cobalt from solution containing 0.107 M $CoSO_4 \cdot 7H_2O$, (b) zinc from solution containing 0.174 M $ZnSO_4 \cdot 7H_2O$, (c) Zn–Co alloy from solution containing 0.107 M $CoSO_4 \cdot 7H_2O$ and 0.174 M $ZnSO_4 \cdot 7H_2O$. Each solution contained 0.14 M Na_2SO_4 and 1.33 M NH_2CH_2COOH. Calculated curves (- - - -) for Co, Zn and H_2.

The partial current densities of each metal and hydrogen during alloy deposition could be calculated by following the method adopted in [5]. The dotted curves in Figure 1 display the partial polarization curves of Co, Zn and H_2 during alloy deposition. The partial polarization curves for the metals differ greatly from the corresponding polarization curves for individual deposition. Codeposition has shifted the potentials of cobalt deposition to more negative values and the potentials of zinc deposition to more positive values. These changes in polarization permit the less noble metal, Zn, to deposit preferentially. This strongly hinders the deposition of Co (i.e., the deposition of Zn–Co alloys belongs to anomalous type). Figure 1 also illustrates that the partial current density of hydrogen is small which implies that the production of alloy has high current efficiency. It is interesting to observe that the shapes of the partial polarization curves in Figure 1 indicate that zinc deposition is limited by charge transfer, while cobalt deposition is limited by transport phenomena.

Figure 2 shows that the cathodic polarization of alloy deposition shifts slightly to more negative values as the

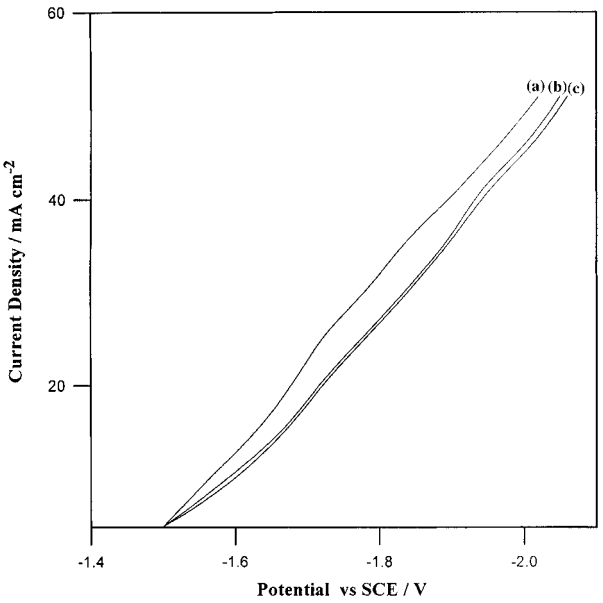

Fig. 2. Galvanostatic cathodic polarization curves for the deposition of Zn–Co alloy on steel at pH 10 and 25 °C from solutions containing 0.107 M $CoSO_4 \cdot 7H_2O$, 0.174 M $ZnSO_4 \cdot 7H_2O$ and 0.14 M Na_2SO_4 and different concentrations of NH_2CH_2COOH: (a) 1.33, (b) 1.60 and (c) 1.86 M.

concentration of glycine increases from 1.33 to 1.86 M. This negative shift is mainly attributed to increasing stability of the Co–glycinate complex species.

Elevating the bath temperature decreases the alloy deposition potential as shown in Figure 3. This behaviour may be attributed to the depolarization effect of temperature on the discharge overpotential of the reducible ions (Co^{2+}, Zn^{2+} and H^+). An increase in temperature enhances hydrogen discharge processes as indicated by cathodic current efficiency (CCE) measurements.

3.2. *Composition of Zn–Co electrodeposited alloy*

Figures 4 to 6 illustrate the cathodic current efficiency (CCE) of Zn–Co alloy and the percentage of zinc in the

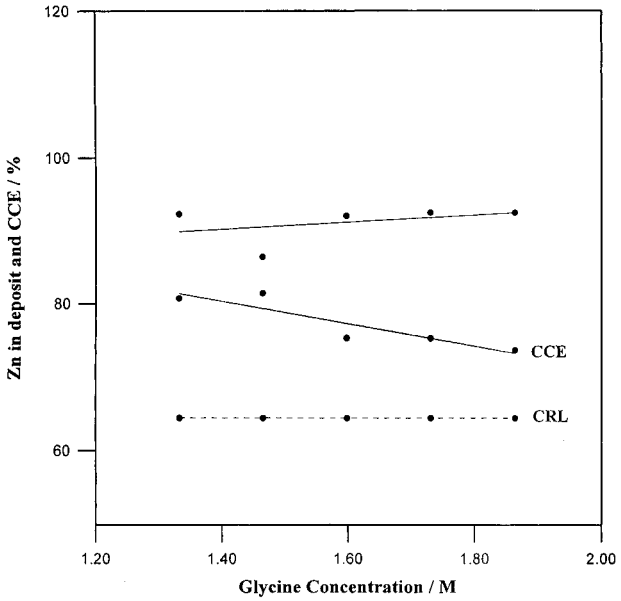

Fig. 4. Effect of NH_2CH_2COOH concentration on CCE and percentage of Zn in the deposits from bath containing 0.107 M $CoSO_4 \cdot 7H_2O$, 0.174 M $ZnSO_4 \cdot 7H_2O$ and 0.14 M Na_2SO_4 at c.d. 0.432 A dm^{-2}, pH 10, time 15 min and 25 °C. CRL represents the percentage of Zn in the bath.

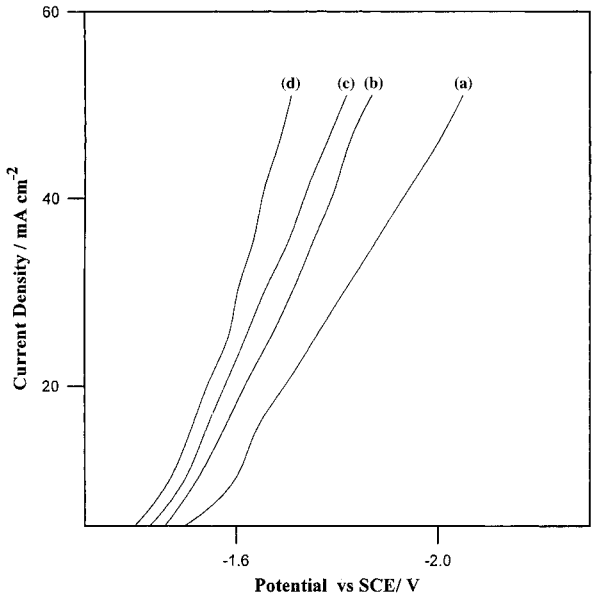

Fig. 3. Galvanostatic cathodic polarization curves for the deposition of Zn–Co alloy on steel from solutions containing 0.107 M $CoSO_4 \cdot 7H_2O$, 0.174 M $ZnSO_4 \cdot 7H_2O$, 0.14 M Na_2SO_4 and 1.33 M, (c)45/(d) NH_2CH_2COOH at pH 10 and at different temperatures: (a) 25, (b) 35 and (c) 55 °C.

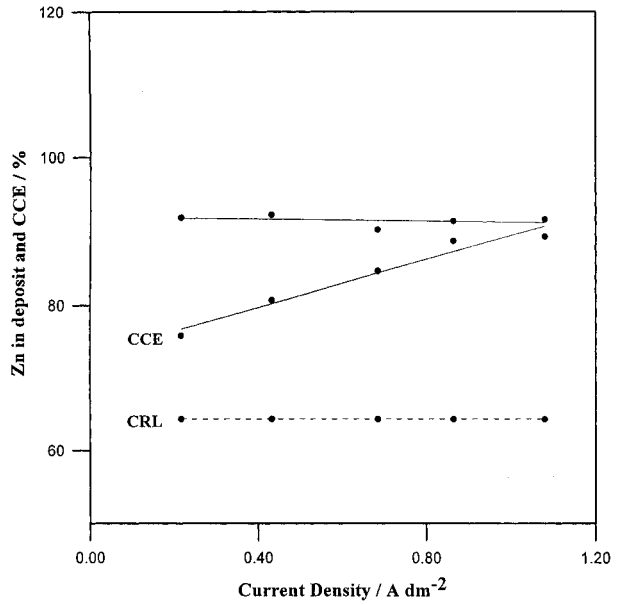

Fig. 5. Effect of current density on CCE and percentage of Zn in the deposits from bath containing 0.107 M $CoSO_4 \cdot 7H_2O$, 0.174 M $ZnSO_4 \cdot 7H_2O$, 0.14 M Na_2SO_4 and 1.33 M NH_2CH_2COOH at pH 10, time 15 min and 25 °C. CRL represents the percentage of Zn in the bath.

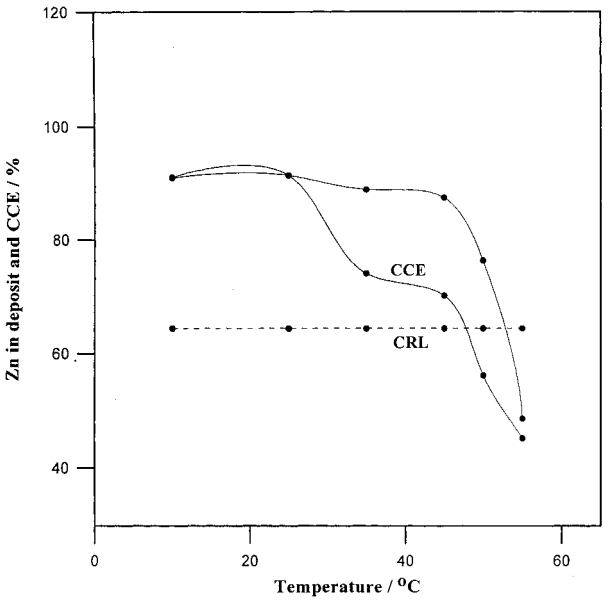

Fig. 6. Effect of temperature on CCE and percentage of Zn in the deposits from bath containing 0.107 M $CoSO_4 \cdot 7H_2O$, 0.174 M $ZnSO_4 \cdot 7H_2O$, 0.14 M Na_2SO_4 and 1.33 M NH_2CH_2COOH at c.d. 0.864 A dm^{-2}, pH 10 and time 15 min. CRL represents the percentage of Zn in the bath.

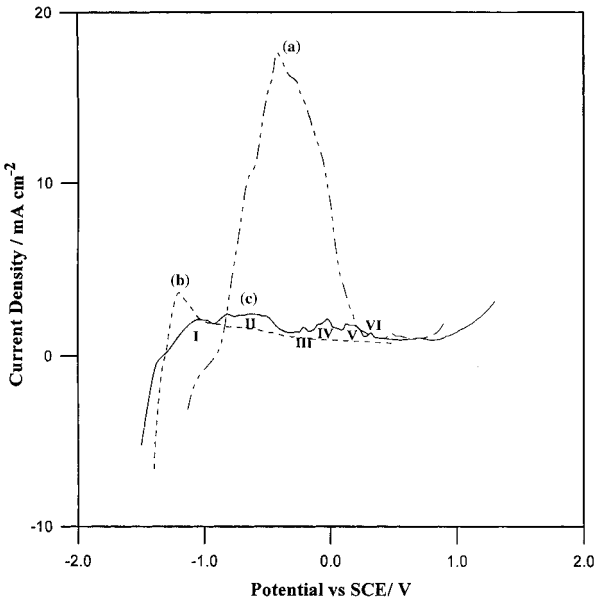

Fig. 7. Linear sweep voltammograms of a fixed glassy carbon electrode in various solutions: (a) 0.107 M $CoSO_4 \cdot 7H_2O$ (deposition potential = −1.3 V vs SCE), (b) 0.174 M $ZnSO_4 \cdot 7H_2O$ (deposition potential = −1.3 V vs SCE), (c) 0.107 M $CoSO_4 \cdot 7H_2O$ and 0.174 M $ZnSO_4 \cdot 7H_2O$ (deposition potential = −1.5 V vs SCE). Each solution containing 0.14 M Na_2SO_4 and 1.33 M NH_2CH_2COOH. Sweep rate 10 mV s^{-1}.

deposit as a function of some plating variables. The label CRL (composition reference line) shows the percentage of Zn in the bath. CCE is less than 100% as a result of simultaneous evolution of hydrogen in all cases studied. The percentage of Zn in the deposits is larger than its percentage in the baths, indicating that the deposition of Zn–Co alloy is of anomalous type [5].

Figure 4 shows that an increase in the glycine concentration tends to increase the percentage of Zn in the deposit slightly and decreases the cathodic current efficiency for Zn–Co deposition. This behaviour is mainly due to an increase in the stability of Co^{2+}–glycinate complex species and consequent inhibition of the reduction of cobalt at the expense of the reduction of hydrogen.

Figure 5 shows the current density dependence of CCE and alloy composition. It can be seen that an increase in current density has no effect on the composition of the deposit but it tends to improve the CCE of the alloy deposition slightly as a result of increasing the cathodic polarization. This assists the discharge of cobalt ions.

The influence of temperature on Zn content in the deposit and on the CCE of alloy deposition is shown in Figure 6. The Zn content in the deposit and the CCE

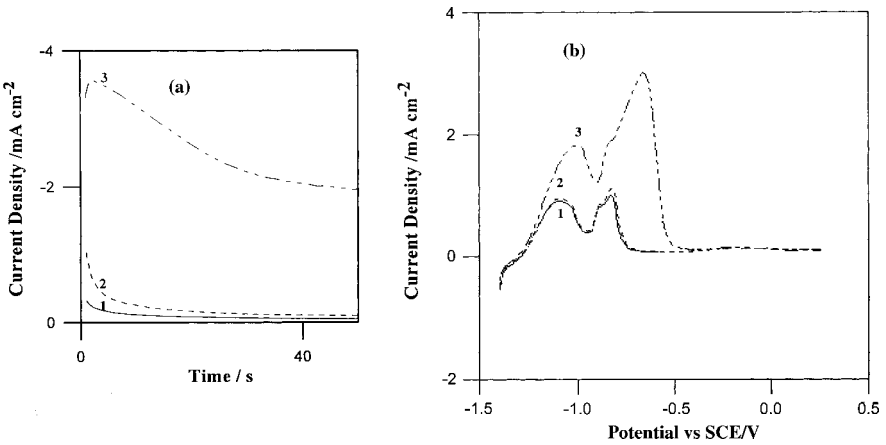

Fig. 8. Potentiostatic j/t transients of deposition (a) and corresponding linear sweep voltammograms of dissolution, (b) of Zn–Co alloy, obtained from solution containing 0.107 M $CoSO_4 \cdot 7H_2O$, 0.174 M $ZnSO_4 \cdot 7H_2O$, 0.14 M Na_2SO_4 and 1.33 M NH_2CH_2COOH. Applied deposition potentials: (a) −0.5, (b) −1.0 and (c) −1.5 V. Sweep rate 10 mV s^{-1}.

of alloy deposition decrease markedly with increasing temperature. The effect of the temperature on the composition of an alloy deposited in anomalous codeposition is determined by two opposing influences: polarization and diffusion. By increasing the temperature, the first effect tends to raise the content of the more noble metal in the deposit, while the second tends to favour the deposition of the less noble. With the plating conditions used in this work, it seems that the influence of polarization predominates over that of diffusion and the cobalt content of the deposits always increases with increasing bath temperature [12]. Consequently, the Zn percentage of the deposit tends to decrease with increasing bath temperature. In the light of the results, anomalous Zn–Co codeposition can be explained in terms of a zinc hydroxide suppression mechanism [3]. Hydrogen evolution and, consequently, a rise in pH in the vicinity of the cathode occurs during electrolysis. If the pH rises sufficiently, precipitation of zinc hydroxide and its adsorption take place on the cathode surface. The hydroxide film prevents Co deposition whereas Zn deposits readily from the adsorbed layer. Therefore, Zn acts as if it were a nobler component of the system. The solubility of the hydroxide film increases with temperature and, as a result, cobalt deposition is accelerated and its content in the deposit increases, Figure 6. The CCE of alloy deposition decreases markedly due to a large decrease in the efficiency of Zn deposition. It is interesting to observe that the curve of Zn content in the deposit cut the CRL at 53 °C, (the temperature at which the Zn content in the deposit is identical with its percentage in the bath). It is clear that below this

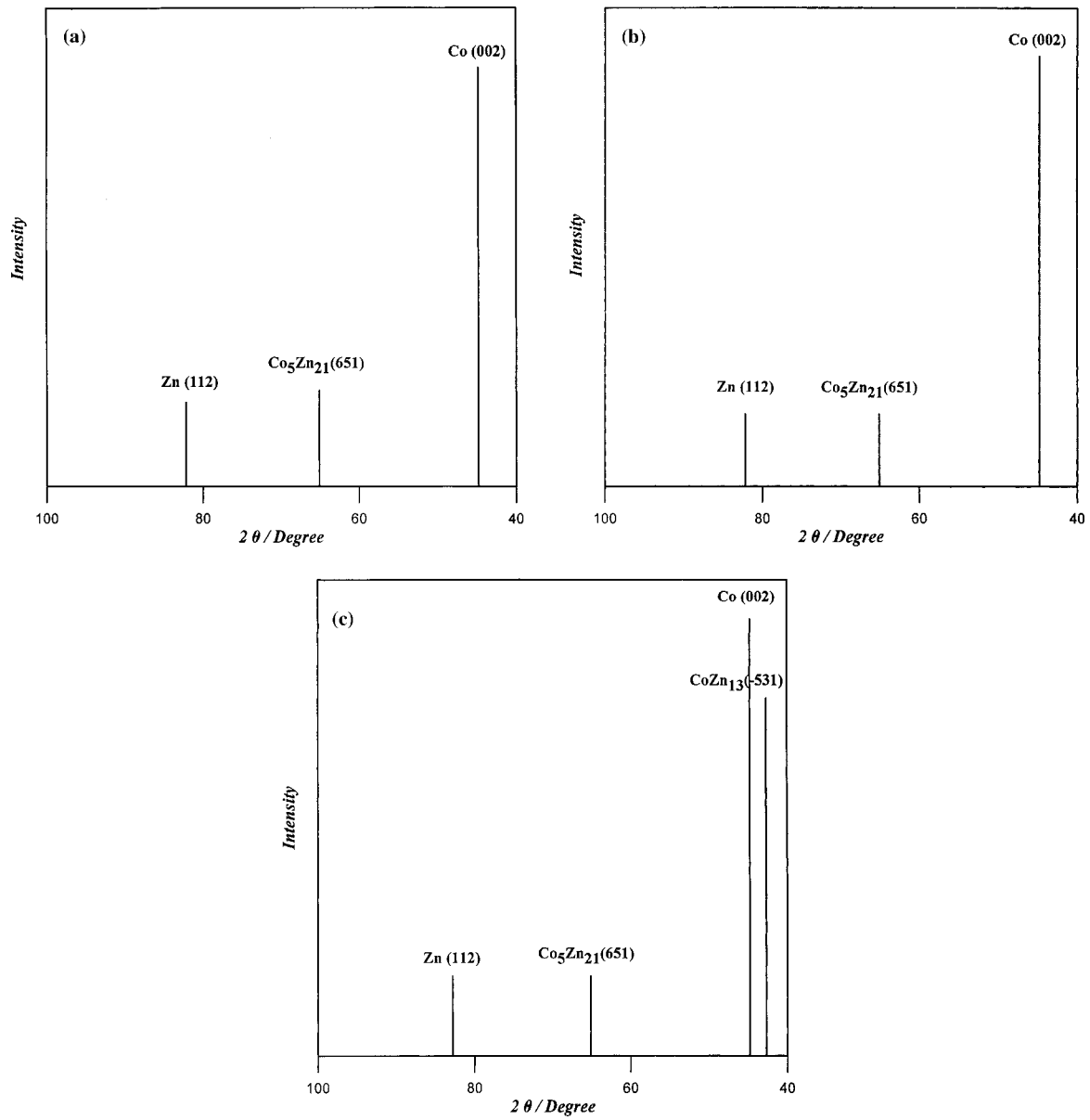

Fig. 9. X-ray diffraction patterns of electrodeposited Zn–Co alloy obtained from a bath containing 0.107 M $CoSO_4 \cdot 7H_2O$, 0.174 M $ZnSO_4 \cdot 7H_2O$, 0.14 M Na_2SO_4 and 1.33 M NH_2CH_2COOH at pH 10, time 15 min, 25 °C and at different current densities: (a) 0.432, (b) 0.864 and (c) 1.080 A dm^{-2}.

temperature, the deposition of Zn–Co alloy is anomalous. The deposition becomes regular above this temperature and a deposit with high cobalt content is obtained.

3.3. *Anodic dissolution of Zn–Co alloy coatings*

To analyse the obtained deposits *in situ*, potentiodynamic stripping (ALSV) was performed. This technique has been shown to be very useful in characterizing the electrodeposited alloy [13]. For this purpose the electrodeposits were obtained potentiostatically under stationary conditions and immediately oxidized by means of voltammetric scan at 10 mV s^{-1}. Figure 7 shows the anodic curves of the dissolution of Co, Zn and Zn–Co alloy coatings. During the dissolution of the Co coating (deposited from an electrolyte containing only Co^{2+}), curve (a), a peak appears on the current – voltage curve at a potential −403 mV vs SCE. On the anodic polarization curve, curve b, obtained during the dissolution of the Zn coating (deposited from an electrolyte containing only Zn^{2+}), a peak appears at a potential −1210 mV vs SCE. During the dissolution of the Zn–Co coating, obtained from an electrolyte containing Zn^{2+} and Co^{2+}, curve (c), six major peaks were detected.

The most anodic peak (peak I) was assigned to the oxidation of pure zinc. Peak II was assigned to the oxidation of zinc in the zinc-rich phase (γ_2-phase) (91–92.8% Zn). Peaks III and IV were assigned to the oxidation of zinc of γ_1(87.4–88.6% Zn) and γ (75.2–85.4% Zn) phase, respectively. Peak V represents the oxidation of a porous cobalt matrix. Finally, peak VI represents the oxidation of pure cobalt. The same result has been reported by others [14–16].

The existence of six peaks on the anodic voltammogram for Zn–Co coating shows that the coatings contain not only Zn and Co separately but also Zn–Co alloy of different content and structure. It can be seen that the Zn–Co alloy is more resistant to corrosion than Zn and Co metals (The dissolution potentials of the alloy are nobler than the individual metals).

Figure 8 shows the potentiostatic j/t transients of the deposition of Zn–Co alloy on glassy carbon electrode from solution containing ions of both metals, Zn and Co. It also shows the corresponding LSVs of dissolution of these alloys in the same solution. The data shows that at all the examined potentials, the LSV possesses only two dissolution peaks. The first peak is assigned to the oxidation of pure zinc while the second is assigned to the oxidation of zinc of γ_2 phase. It is obvious from Figure 8 that when the applied potential is −0.5 V, the corresponding voltammogram possesses two oxidation peaks, one of them is for pure zinc. This means that Zn is deposited on glassy carbon at a more positive potential than its equilibrium potential (−0.763 V). This indicates that zinc shows underpotential deposition (UPD). UPD Zn may inhibit either the formation of cobalt clusters by deposition on the substrate or the growth of clusters by interaction with growing cobalt clusters. This inhibition enhances the polarization of Co deposition at constant current density and amplified the primary electrode potential in causing anomalous deposition.

The anomalous codeposition of Zn–Co alloys from glycinate baths may be attributed to underpotential deposition of zinc and the zinc hydroxide suppression mechanism.

3.4. *Microstructure of the electrodeposits*

X-ray diffraction measurements were carried out on Zn–Co electrodeposits from selected baths and under different experimental conditions. X-ray diffraction studies revealed that the phase structure of the deposits was controlled by the applied current density. At low current density, the deposit was composed mainly of a cubic Co_5Zn_{21}. However, at high current density, it consisted mainly of cubic Co_5Zn_{21} [ASTM cards, 22 - 0521] and monoclinic Co Zn_{13} [ASTM cards, 29 - 0523] phases.

Table 1. X-ray diffraction data for the electrodeposited Zn–Co alloy obtained from a bath containing 0.107 M $CoSO_4 \cdot 7H_2O$, 0.174 M $ZnSO_4 \cdot 7H_2O$, 0.14 M Na_2SO_4 and 1.33 M NH_2CH_2COOH
Conditions: pH 10, deposition time 15 min, temperature = 25 °C and at different current densities

Current density /A dm^{-2}	Alloy composition /%	2θ	d /Å	$h\ k\ l$	Phase	Structure	Lattice parameters /Å		
							a	b	c
0.432	Zn_{92}–Co_8	44.80	2.0212	(002)	Co	HCP	2.505	2.505	4.060
		65.10	1.4315	(651)	Co_5Zn_{21}	cubic	11.27	11.27	11.27
		82.20	1.1717	(112)	Zn	hexagonal	2.665	2.665	4.950
0.864	Zn_{91}–Co_9	44.80	2.0212	(002)	Co	HCP	2.505	2.505	4.060
		65.10	1.4315	(651)	Co_5Zn_{21}	cubic	11.27	11.27	11.27
		82.20	1.1717	(112)	Zn	hexagonal	2.665	2.665	4.950
1.080	Zn_{89}–Co_{11}	42.70	2.1156	(−531)	$CoZn_{13}$	monoclinic	13.30	7.535	4.992
		44.80	2.0212	(002)	Co	HCP	2.505	2.505	4.060
		65.10	1.4315	(651)	Co_5Zn_{21}	cubic	11.27	11.27	11.27
		82.20	1.1717	(112)	Zn	hexagonal	2.665	2.665	4.950

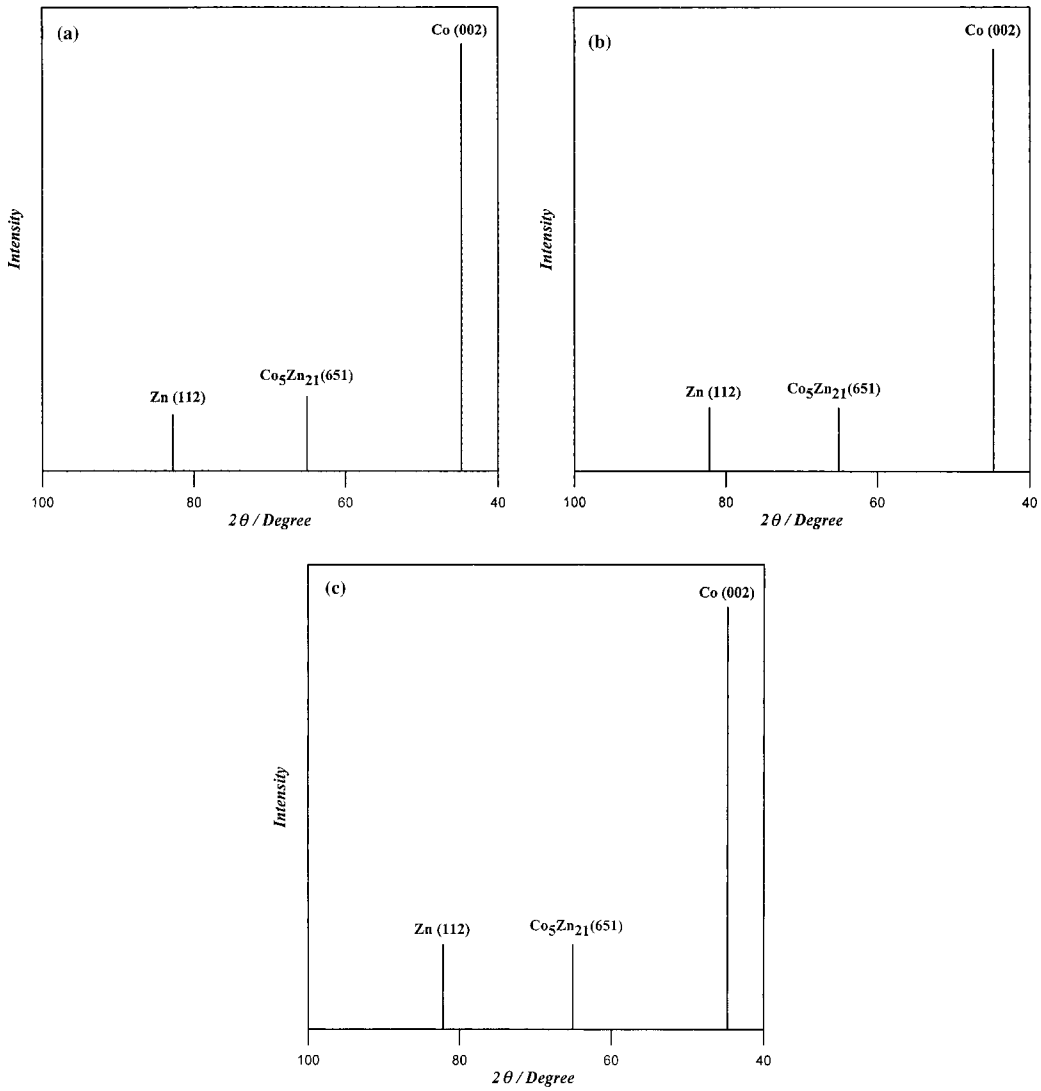

Fig. 10. X-ray diffraction patterns of electrodeposited Zn–Co alloy obtained from a bath containing 0.107 M $CoSO_4 \cdot 7H_2O$, 0.174 M $ZnSO_4 \cdot 7H_2O$, 0.14 M Na_2SO_4 and 1.33 M NH_2CH_2COOH at c.d. 0.864 A dm^{-2}, pH 10, time 15 min, and at different temperatures: (a) 10, (b) 25 and (c) 55 °C.

Table 2. X-ray diffraction data for the electrodeposited Zn–Co alloy obtained from a bath containing 0.107 M $CoSO_4 \cdot 7H_2O$, 0.174 M $ZnSO_4 \cdot 7H_2O$, 0.14 M Na_2SO_4 and 1.33 M NH_2CH_2COOH.
Conditions: current density 0.864 A dm^{-2}, pH 10, deposition time 15 min and at different temperatures.

Temp. /°C	Alloy composition /%	2θ	d /Å	$h\ k\ l$	Phase	Structure	Lattice parameters /Å		
							a	b	c
10	Zn_{92}–Co_8	44.80	2.0212	(002)	Co	HCP	2.505	2.505	4.060
		65.10	1.4315	(651)	Co_5Zn_{21}	cubic	11.27	11.27	11.27
		82.20	1.1717	(112)	Zn	hexagonal	2.665	2.665	4.950
25	Zn_{91}–Co_9	44.80	2.0212	(002)	Co	HCP	2.505	2.505	4.060
		65.10	1.4315	(651)	Co_5Zn_{21}	cubic	11.27	11.27	11.27
		82.20	1.1717	(112)	Zn	hexagonal	2.665	2.665	4.950
55	Zn_{48}–Co_{52}	44.80	2.0212	(002)	Co	HCP	2.505	2.505	4.060
		65.10	1.4315	(651)	Co_5Zn_{21}	cubic	11.27	11.27	11.27
		82.20	1.1717	(112)	Zn	hexagonal	2.665	2.665	4.950

X-ray diffractograms of the Zn–Co alloys obtained at different current densities indicated the presence of pure cobalt and zinc, (Figure 9 and Table 1). The data indicated that the Co_5Zn_{21} phase has a preferred orientation of (651). This appeared in all examined deposits but with different intensities. At high current density, a new phase, Co Zn_{13} was formed with Miller indices (−531).

Increasing the temperature of the bath from 10 to 55 °C had no significant effect on the intensity of the planes, (651) and (112) but it tended to decrease the intensity of (002) plane, (Figure 10 and Table 2).

4. Conclusions

Bright deposits of Zn–Co alloy can be electrodeposited onto steel substrates from glycinate baths. The effect of some plating variables on the cathodic current efficiency, composition and structure of the alloy deposits was studied. An explanation has been offered for the various trends observed in the light of cathodic polarization. The potentiodynamic dissolution of coatings illustrates that the coatings contain not only Zn and Co but also Zn–Co alloy of different content and structure. The anomalous codeposition of Zn–Co alloy may be attributed to underpotential deposition of Zn and Zn hydroxide suppression.

References

1. P-Y. Chen and I-W. Sun, *Electrochim. Acta* **46** (2001) 1169.
2. E. Grunwald, A. Ziman, Cs. Varhelyi and Cs. Juhos, *Galvanotechnik* **85** (1994) 327.
3. A. Stakeviciute, K. Leinartas, G. Bikulcius, D. Virbalyte, A. Sudavicius and E. Juzeliunas, *J. Appl. Electrochem.* **28** (1998) 89.
4. I. Kirilova, I. Ivanov and St. Rashkov, *J. Appl. Electrochem*, **27** (1997) 1380.
5. A. Brenner, 'Electrodeposition of Alloys', Vol. 1 (Academic Press New York, 1963).
6. Y. Okuda and K. Himatsu, *Jpn. Kokai Tokkyo Koho*, *Jp. 05. 179*, *481* (*95. 179*, *481*), (Cl. C25D3/56), 20 July 1993, Appl. 91/ 360, 157 (27 Dec. 1991).
7. R. Fratesi, G. Roventi, G. Giuliani and C.R. Tomachuk, *J. Appl. Electrochem.* **27** (1997) 1088.
8. S.S. Abd El-Rehim, M.A.M. Ibrahim, S.M. Abd El-Wahab and M. Dankeria, *Trans. Inst. Finish.* **77**(1) (1999) 31.
9. Z. Tu, J. Zhang, W. Li, Z Yang and M. An, *Trans. Inst. Met. Finish.* **73**(2) (1995) 48.
10. V. Narasimhamurthy and B.S. Sheshadri, *Met. Finish.* **96**(4), (1998) 24.
11. S.S. Abd El-Rehim, S.A. Refaey, G.S. Gebel, F. Taha and M.B. Saleh, *J. Appl. Electrochem.* **25** (1995) 1.
12. R. Albalat, E. Gomez, C. Muller, J. Pregonas, M. Sarret and E. Valles, *J. Appl. Electrochem.* **21** (1991) 44.
13. A.R. Despic and V.D. Jovic, 'Modern Aspects of Electrochemistry' (Plenum, New York, 1995).
14. E. Gomez and E. Valles, *Current Topics in Electrochem.* **4** (1997) 195.
15. M. Hansen, 'Constitution of Binary Alloys' (McGraw-Hill, New York, 1958), p. 520.
16. E. Gomez and F. Valles, *J. Electroanal. Chem.* **421** (1997) 157.